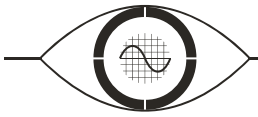

Lehrstuhl für Bildverarbeitung
Institute of Imaging & Computer Vision

Application of Supervised Range-Constrained Thresholding to Extract Lung Pleura for Automated Detection of Pleural Thickenings from Thoracic CT Images

K. Chaisaowong, A. Knepper, T. Kraus, and T. Aach
Institute of Imaging and Computer Vision
RWTH Aachen University, 52056 Aachen, Germany
tel: +49 241 80 27860, fax: +49 241 80 22200
web: www.lfb.rwth-aachen.de

in: Proc. SPIE Medical Imaging: Computer-Aided Diagnosis.
See also BibTeX entry below.

BibTeX:

```
@inproceedings{CHA07a,
  author      = {Kraisorn Chaisaowong and Achim Knepper and Thomas Kraus and Til Aach},
  title       = {Application of Supervised Range-Constrained Thresholding to Extract Lung Pleura for
                 Automated Detection of Pleural Thickenings from Thoracic {CT} Images},
  booktitle   = {Proc. SPIE Medical Imaging: Computer-Aided Diagnosis},
  editor      = {Maryellen L. Giger and Nico Karssemeijer},
  address     = {San Diego, CA},
  volume      = {6514},
  pages       = {65143M},
  month       = {February 17--22,},
  year        = {2007},
}
```


document created on: April 11, 2007
created from file: CHA07a.tex
cover page automatically created with CoverPage.sty
(available at your favourite CTAN mirror)

RWTH AACHEN
RHEINISCH-WESTFÄLISCHE TECHNISCHE HOCHSCHULE AACHEN

Application of Supervised Range-Constrained Thresholding to Extract Lung Pleura for Automated Detection of Pleural Thickenings from Thoracic CT Images

K. Chaisaowong*[a,b], A. Knepper[a], T. Kraus[c], and T. Aach[a]
[a]Institute of Imaging & Computer Vision,
RWTH Aachen University, Templergraben 55, 52056 Aachen, Germany;
[b]The Sirindhorn International Thai-German Graduate School of Engineering,
King Mongkut's Institute of Technology North Bangkok, 10800 Bangkok, Thailand;
[c]Institute and Out-Patient Clinic for Occupational Medicine,
University Hospital Aachen, Pauwelsstraße 30, 52074 Aachen, Germany

ABSTRACT

We develop an image analysis system to automatically detect pleural thickenings and assess their characteristic values from patients' thoracic spiral CT images. Algorithms are described to carry out the segmentation of pleural contours and to find the pleural thickenings. The method of thresholding was selected as the technique to separate lung's tissue from other. Instead thresholding based only on empirical considerations, the so-called "supervised range-constrained thresholding" is applied. The automatic detection of pleural thickenings is carried out based on the examination of its concavity and on the characteristic Hounsfield unit of tumorous tissue. After detection of pleural thickenings, in order to assess their growth rate, a spline-based interpolation technique is used to create a model of healthy pleura. Based on this healthy model, the size of the pleural thickenings is calculated. In conjunction with the spatio-temporal matching of CT images acquired at different times, the oncopathological assessment of morbidity can be documented. A graphical user interface is provided which is also equipped with 3D visualization of the pleura. Our overall aim is to develop an image analysis system for an efficient and reliable diagnosis of early stage pleural mesothelioma in order to ease the consequences of the expected peak of malignant pleural mesothelioma caused by asbestos exposure.

Keywords: malignant pleural mesothelioma; thoracic spiral CT; computer-assisted diagnosis; feature extraction; supervised range-constrained thresholding; lung pleura; pleural thickenings; computer-generated 3D imaging.

1. INTRODUCTION

1.1 Malignant Pleural Mesothelioma

Mesothelioma is a usually malignant tumor of mesothelial tissue, e.g. of that of the pleura. It is statistically documented that 70-90% of malignant pleural mesothelioma can be traced back to asbestos exposure [1, 2]. After a statutory prohibition in the year 1993 in Germany to use asbestos, occurrence of malignant pleural mesothelioma morbidity and mortality in Germany is expected to peak during 2010s, due to the long latency period of - on the average - 35 years.

1.2 Current Investigation Program in Germany

In Germany, an assessment program is applied to asbestos exposed persons. Besides a lung function test, a typical non-invasive diagnosis based on thoracic axial CT images (Figure 1) is also included in this assessment program. Depending on the layers' thickness, the number of images varies between 80 slices with a thickness of 5 mm to about 700 slices with a thickness of 0.5 mm. Physicians view each slice on a workstation in order to find pleural thickenings. The diagnostic findings are documented in a standardized form containing data such as their size, position, and growth rate [3].

* Kraisorn.Chaisaowong@lfb.rwth-aachen.de;
Phone +49 241 80-27862; Fax +49 241 80-22200; http://www.lfb.rwth-aachen.de/en/projects/pleuramesothelioma/

1.3 Motivation

This visual diagnostic approach is a very time consuming procedure, taking about 20 to 30 minutes per data set, and is considered as being often subjective, since differences in the diagnostic results between different investigating clinicians do occur [4]. To increase the accuracy of the localization and of the topological information of these quite small image regions within a subjective visual evaluation, an even longer investigating time would be needed for each data set. However, due to the increasing number of investigations and high work load of the physicians involved, this solution is not practicable. Therefore, a method is needed to provide a more accurate assessment of pleural mesothelioma at an early stage, which is reliable, consistent, and reproducible.

After diagnosis of malignant pleural mesothelioma, survival time was documented to be between 4 to 18 months without any therapy [5]. For early stage pleural mesothelioma, however, pleurectomy together with perioperative treatment can reduce the morbidity and delay the mortality [6]. Thus, efficient and reliable diagnosis of early stage pleural mesothelioma is a key factor to ease the consequences of the expected peak of malignant pleural mesothelioma. The aim of this work is to develop a computer system to automatically detect and quantitatively assess pleural thickenings in axial thoracic CT images.

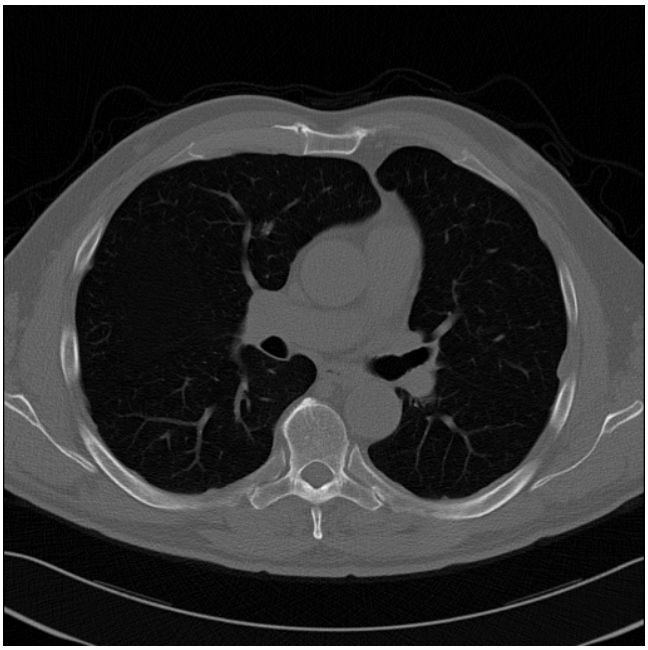

Fig. 1. Original thoracic CT image of an asbestos exposed patient.

2. METHODS

2.1 Algorithm steps

We have developed an image analysis system to automatically detect and assess pleural thickenings in thoracic CT images of asbestos exposed patients, in order to diagnose already the early stage of pleural mesothelioma [7,8,9]. The algorithms behind it can be described in six steps as follows.

1. Segmentation of pleural contours

An appropriate method to determine a threshold is employed to separate lung tissue from another tissue [10]. Spurious remaining artifacts are eliminated by applying a morphological opening three times followed by two applications of a closing, both with a 3×3 structure element [11]. In addition to the sought lung boundaries, the contour computation algorithm also yields a variety of other closed contours, such as those of other, vessel-related regions, and the edges of the patient table. By means of the bounding box, those two closed contours whose bounding box areas form the largest pair are identified as the pleural contours.

2. Detection of pleural thickenings

The contour of healthy pleura as computed up to this stage can be modeled as being convex shaped. The QuickSort algorithm is employed to find the convex hull. Candidate pleural thickenings are locally concave deviations from the convex hull [12], which can be found by calculating the difference between the convex hull and the existing contour.

3. Identification of pleural thickenings

The above procedures provide a set of candidates for pleural thickenings. A candidate thickening can only form a pleural thickening if it extends over at least three slices, and only if 10 percent of its pixels, lying within the contour, exhibit a Hounsfield unit larger than a given threshold for this purpose, which separates genuine pleural thickenings from fat (Figure 2).

4. Assessment of characteristic properties

The pleural contour is interpolated at those locations where a pleural thickening was detected to provide a local model of the healthy pleura contour. The interpolation is based on a second order spline model [13]. Integration of these volumes over the layers involved yields the total volume of each pleural thickening.

5. Spatio-temporal matching

Oncopathological assessment of the growth of pleural thickenings of a patient requires that axial CT data sets from the same patient, but taken at different times, have to be matched (or registered) with each other. This step, which will be implemented in future, seeks to provide a semi-automatic matching of anatomic structure recorded at different times, so that a pleural thickening can be traced over time. For this purpose, the anatomical matching of significant landmarks such as the position of Carina tracheae, the centre of Processus spinosus, and corners of lungs will be carried out manually to calculate the transformation matrices.

6. 3D Visualization of pleural thickenings

The segmented pleura is approximated by triangulation invoking the “Marching Cubes” algorithm and can be visualized as a 3D object [14].

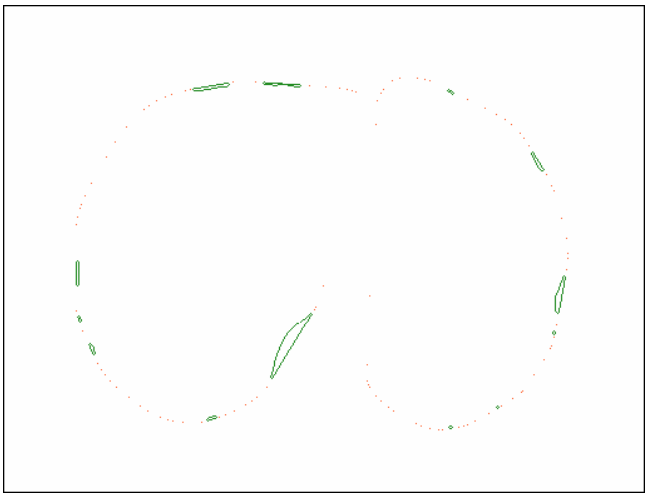

Fig. 2. Pleural thickenings detected as concave differences from the convex hull. Note that the classification algorithm in its present form does not utilize information about the position of the detected pleural thickenings, which leads to misclassifications of a concave area near the spinal cord and along the mediastinum and bronchus.

2.2 Lung Segmentation by Thresholding

As mentioned above, thresholding is applied to separate the lung tissue from other areas in the thoracic CT image, with the aim of automatic detection of the pleura contours of lung lobes. Until now, the determination of an appropriate threshold for this step was based on the empirical considerations that, in our data sets, lung tissue with Hounsfield units in the range between -180 to -910 HU is reasonably well separated from other, surrounding tissues such as fat ranging between -50 to -220 HU [15]. A first estimate of the lung areas was then obtained by thresholding at the empirical value of -550 HU.

However, in order to improve the reliability and the robustness of the algorithm, an approach based on a novel technique, the supervised range-constrained thresholding, is applied instead of the former empirical estimation. Guided by data examples, *a priori* knowledge of these examples was integrated into the threshold computation. The method consists in details of three steps, which will be described as following.

2.3 Supervised Range-Constrained Thresholding

1. Basic Approach

Thresholding, as a homogeneous point operation, is a segmentation technique widely applied in several fields of image processing [16]. The threshold is used to separate an image into, in generally, two regions. Considering a two-dimensional data set $f(\vec{x})$ with L gray levels, where $f(\vec{x})$ is the data at position $\vec{x}$, thresholding can be regarded as a mapping from gray levels or other features to class labels. For a two-level thresholding, a threshold θ determines the clas label $C(\vec{x})$ at every position of the data set into the object class C_O and the background class C_B. The thresholding operation is then defined as follows:

$$C(\vec{x}) = \begin{cases} C_O & f(\vec{x}) > \theta \\ C_B & else \end{cases} \tag{1}$$

Naturally, classification errors will occur. In this two-class decision problem, two error types are distinguished. The first type are false negatives, which wrongly assign object points to the background class. The other error type are false positives. This error classifies background pixels into the object class. An ideal threshold shall minimize a criterion related to both types of classification errors.

2. Supervision-Based Approach for Threshold Selection

In the above mapping, increasing the threshold causes the false negative error to increase, since more object elements are then classified as background. Thus the false negative error is a monotonically increasing function of the threshold. Similarly, decreasing the threshold causes an increase of the false positive error, since more background elements are then classified as object. Thus, the threshold must lie in a certain range to keep both types of classification errors [10,17] sufficiently small. In others words, the threshold shall not be smaller than a lower bound H_{LB}^{B}, since then the false positive error would become too large. On the other hand, the threshold shall not exceed an upper bound H_{UB}^{B}, since otherwise the false negative error will become too large. The *a priori* knowledge to confine the range of threshold is derived from the frequency distribution or histogram of the background itself. In order to determine an appropriate threshold guided by the background frequency distribution, the following steps are to be done.

a. The region of interest, in which the object is present, is to be determined.

b. Estimate the proportion of the background area to the area of the region of interest, and then find the minimal and maximal value of the background area proportion to determine the corresponding histogram interval.

c. Determine the sought threshold lying between the boundary thresholds by seeking the best separation within this interval.

3. Estimation of the Proportion of the Background Area

Before the determination of the associated lower and upper threshold bounds, the background frequency distribution has to be estimated first. The estimation can be done in mainly three ways [10]:

- *A Ground Truth* can be used to calculate the boundary parameters, if a number of sample data set with ground truths is available.
- *Prior knowledge* on an individual image can be used to approximate the two parameters, when sample images with ground truth are not available.
- *Visual judgment* is the sole method, when neither ground truth nor prior knowledge was available. The estimation of parameters can be facilitated by using the macro pixel [10].

4. Supervised Range-Constrained Least Valley Detection

For reasonably selected error bounds, the boundary thresholds will be located near a valley of the corresponding histogram (Figure 3) [10,18], which is assumed to separate the two different regions, i.e. object and background. The decision threshold is thus determined by the valley within the interval. In order to determine the boundary thresholds and the final decision threshold via the least valley-approach, the following steps are carried out:

a. Calculation of the cumulative histogram of the data set $H(i)=\sum_{n=0}^{i} h(n)$ with $h(n)$ representing the histogram of feature $n=0,\ldots,L$.

b. Determine r_{low}, which is the data value corresponding to the background lower bound H_{LB}^{B}:

$$r_{low}=\min_{i}\left\{i \mid H(i)\geq H_{LB}^{B}\right\}. \tag{2}$$

c. Determine r_{high}, which is the data value corresponding to the background upper bound H_{UB}^{B}:

$$r_{high}=\max_{i}\left\{i \mid H(i)\leq H_{UB}^{B}\right\}. \tag{3}$$

d. Evaluate the histogram entry of each data value between the above bounds $[r_{low}, r_{high}]$ by calculating the relative deviation d_{rel} of the cumulative histogram with the usage of an appropriate subinterval width ∂I:

$$d_{rel}(i)=\frac{H(i)-H(i-\partial I)}{\partial I}, \tag{4}$$

by substitution of ∂I with the finest incremental step value, the relative deviation becomes step-wise deviation:

$$d_{rel}(i)=\frac{H(i)-H(i-1)}{1}=d(i), \tag{5}$$

the step-wise deviation $d(i)$ is hence equal to the value of the histogram:

$$d(i)=h(i). \tag{6}$$

e. Find the minimum of these histogram entries and thence the threshold:

$$\theta_{SRCLVD}=i_{\min}\big|_{\min\{h(i)\}}. \tag{7}$$

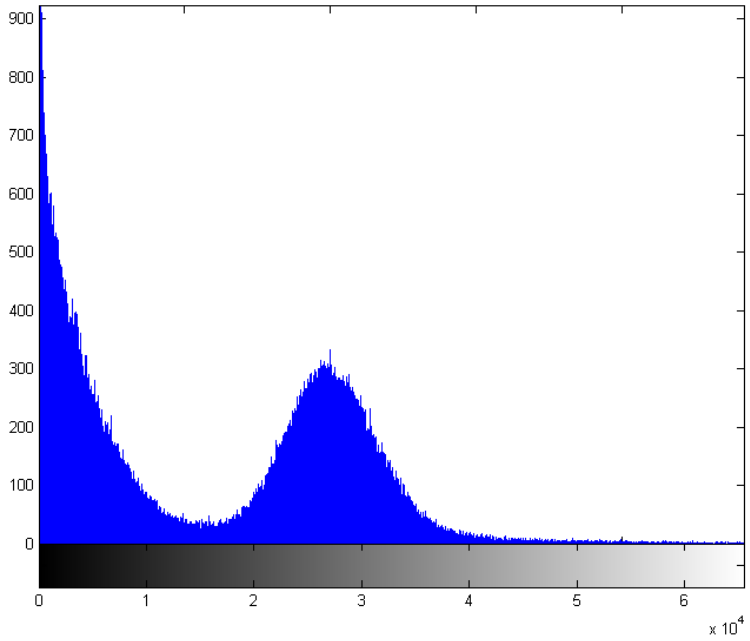

Fig. 3. A histogram from an original thoracic CT image, ranging from 0 to 65,535.

3. RESULTS

3.1 Application Steps

In order to test the reliability and the robustness of the algorithm, the described technique was applied both to find the region of interest and the lung area itself. We define the whole thorax in each slice as region of interest. Hence, the supervised range-constrained thresholding algorithm had to find the thorax out of the whole image, which includes also the edges of CT system table seen in several CT slices. After thresholding, a method of bounding box was used to find the largest region within the binary result. The region with the largest bounding box was considered to be the thorax, which is the region of interest fed forward to the second step.

The second step was to detect the lung area within the thorax. Since the lung area has lower Hounsfield values than that of the connective tissue and blood vessels contained in the thorax, the reverse threshold was applied in this case. After binary thresholding, a pair of regions was sought, whose bounding boxes form the largest pair. Those two regions were then identified as the lung area.

3.2 Estimation of Parameters

To confine the background area, slices were analyzed. The estimation of the two parameters needed was in our case based on visual judgment. In order to estimate the parameters for both steps, a number of slices were viewed. The slices were selected such as to achieve the estimation results for the lower and upper bound of the proportion of background area, which cover existing data. Manual segmentation was performed to quantify the proportion of the background area to the area of the region of interest. The background and the region of interest were then separately labeled to create a binary image. Figure 4 shows the originals of two CT slices and the binary supervised segmentations to determine the upper and lower bounds of the background proportion to the thorax as the region of interest. Figure 5 shows the binary supervised segmentation to determine the upper and low bound of the background proportion to the lungs as the sought object. Based on these random selected CT slices, the values for the parameters shown in Table 1 are were obtained.

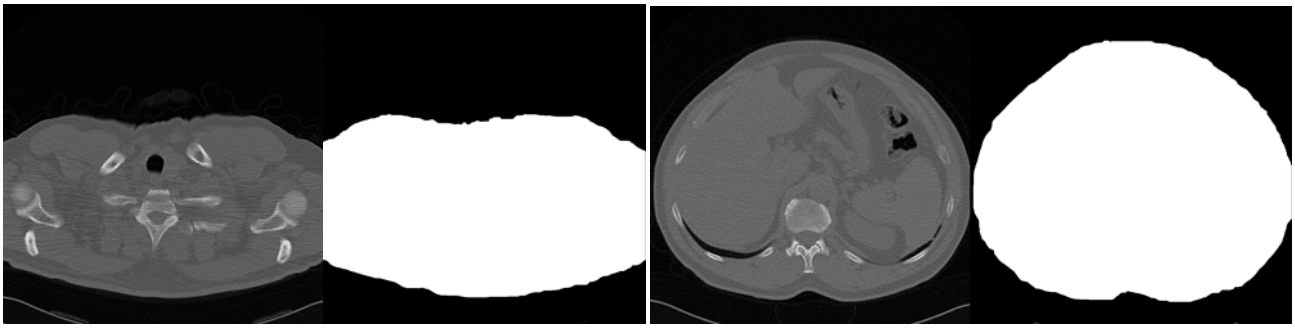

Fig. 4. Two samples after manual segmentation to estimate the lower and upper bound of the proportion of the background area with the thorax as the region of interest.

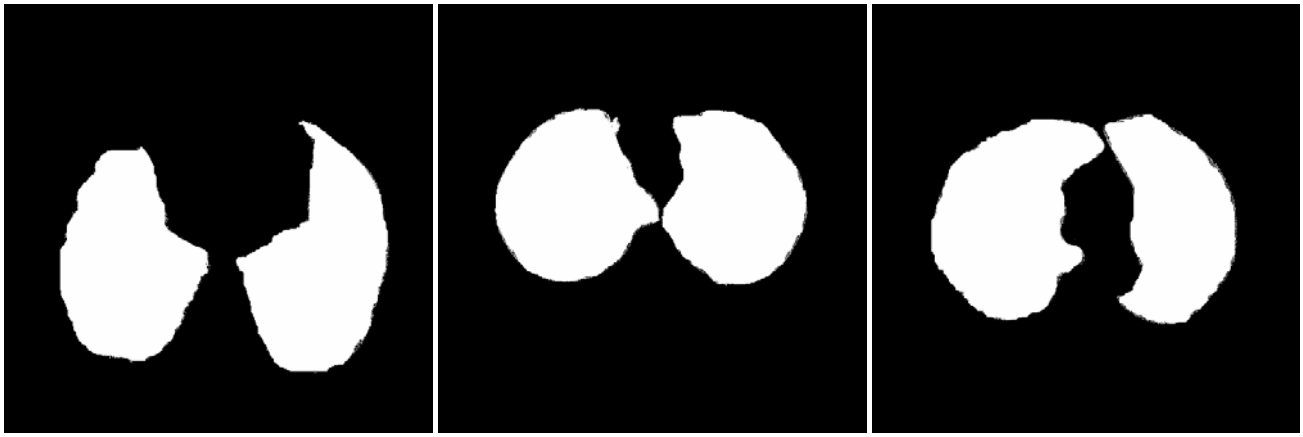

Fig. 5. Three samples after manual segmentation to estimate the lower and upper bound of the proportion of the background area with the lung area within a slice as the region of interest of the final step.

Tab. 1. Supervision parameters to constrain the range of background proportion to sought object.

	Lower bound H_{LB}^{B}	Upper bound H_{UB}^{B}
Parameters to detect thorax	0.5045	0.6494
Parameters to detect lungs	0.3319	0.4653

3.3 Results of Thresholding

Figure 6 shows the results from four original CT slices. Slices are randomly selected from the middle part of the thorax, i.e. slices within the range of 15% to 85% of the total number of each CT data set. Figures on the left side show the results after the application of the supervised range-constraint thresholding to detect the thorax in the original CT slices as the region of interest for the next step. In the thorax of some slices, bronchi remain as a large area close to the lung, whereas large vessels can be found as connective tissue within the lungs.

The right-hand side of Figure 6 shows the results after the application of supervised range-constrained thresholding to detect the lungs within the thorax. As the input of this algorithm step, results from the last step were taken. All results show that the lungs were detected correctly.

Figure 7 shows the results for slices in which the lung areas are very close to each other.

Figure 8 shows thresholding results of two CT slices. The upper and lower left pictures show the results after the application of the constrained thresholding technique to detect the thorax. The whole thorax within the slice was detected correctly. After detection of the thorax, the result was fed forward to detect the lung area. The upper and lower right

pictures show the results after the application of constrained thresholding to detect the lung area. In this case, certain large vessels within the lung were not included into the detected lung tissue.

Fig. 6. Left: Results after thorax detection. Right: Results after the detection of the lungs. Both the thorax and lungs were detected correctly.

Fig. 7. Left: Results after thorax detection. Right: Results after the detection of the lungs. Both the thorax and lungs were detected correctly. Two close lungs can be also separated correctly.

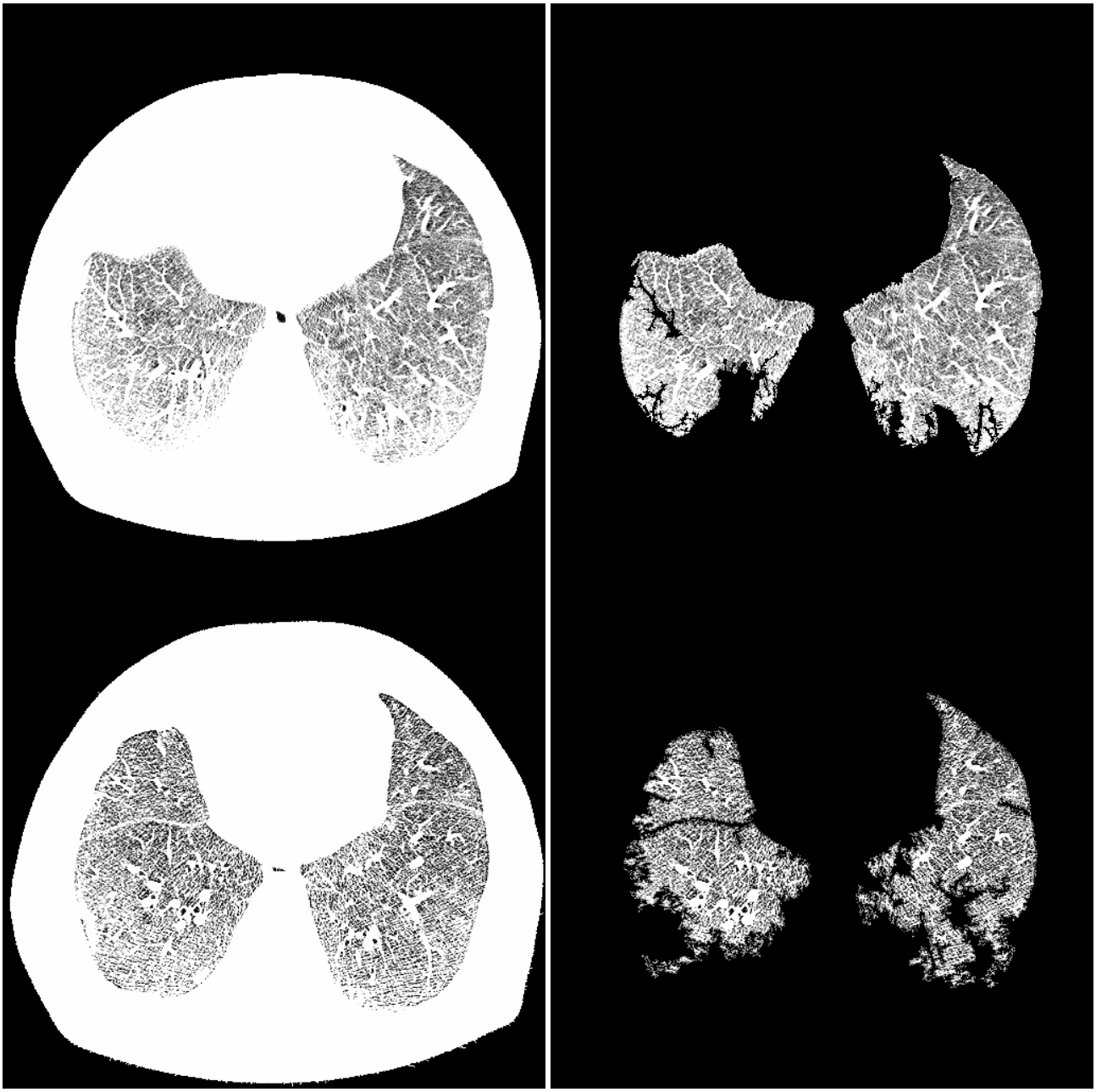

Fig. 8. Left: Results after thorax detection. Right: Results after the detection of the lungs. In both slices, some large vessels were not included into the connected lung tissue.

4. CONCLUSIONS

In this paper, we described parts of the development of an image analysis system concerning an approach to separate the lung tissue from other areas within the thoracic CT image, in order to automatically detect the pleura contours of lung lobes. The technique is based on thresholding. In the former version, threshold determination was based on the empirical considerations that Hounsfield units of lung tissue ranging between -180 to -910 HU are reasonably well separated from other surrounding tissues such as fat with Hounsfield value between -50 to -220 HU. A first estimate of the lung areas was obtained by thresholding at -550 HU.

In order to improve the reliability and the robustness of the software system, a recent approach based on supervised range-constrained thresholding is applied. This method consists of three steps. First, the region of interest has to be determined in the image. The histogram of the region of interest is used under supervision to estimate the frequency range in which the region of interest and the background vary. Finally, the threshold is determined by minimum histogram valley.

REFERENCES

1. O. Hagemeyer, H. Otten, and T. Kraus, "Asbestos consumption, asbestos exposure and asbestos-related occupational diseases in Germany," *Int Arch Occup Environ Health*. 79(8):613–620, 2006.
2. H. J. Raithel, T. Kraus, K. G. Hering, and G. Lehnert, "Asbestbedingte Berufskrankheiten: Aktuelle arbeitsmedizinische und klinisch-diagnostische Aspekte," *Deutsches Ärzteblatt*, 93(11):A685–A693, 1996.
3. K. Hering and T. Kraus, "Coding CT-classification in occupational and environmental respiratory disease (OERD)," *International Classification of HRCT for Occupational and Environmental Respiratory Diseases*, Springer, Tokyo, pp 15-23, 2005.
4. T. M. I. Carl, "Interreadervarianz bei der HRCT- und CXR-Befundung in einer Längsschnittstudie bei ehemals asbeststaubexponierten Personen," *Doctoral Thesis*, Medizinische Fakultät, RWTH Aachen, 2004.
5. S. Sohrab, M. Hinterthaner, G. Stamatis, K. Rödelsperger, H.J. Woitowitz, and N. Konietzko, "Das maligne Pleuramesotheliom," *Deutsches Ärzteblatt*, 97(48):A3257–A3262, 2000.
6. M. Pistolesi and J. Rusthoven, "Malignant pleural mesothelioma: Update, current management, newer therapeutic strategies," *Chest*. 126(4):1318-1329, 2004.
7. S. Vogel, T. Klein, D. Meyer-Ebrecht, and T. Kraus, "Ein Bildverarbeitungssystem für die automatisierte Vermessung und quantitative Verlaufsdokumentation von pleuralen Verdickungen," in Proc. *Workshop Bildverarbeitung für die Medizin 2004 Algorithmen - Systeme - Anwendungen*, Berlin, pp 433-437, 2004.
8. P. Jäger, S. Vogel, A. Knepper, T. Kraus, and T. Aach, "3D-Erkennung, Analyse und Visualisierung pleuraler Verdickungen in CT-Daten," in Proc. *Workshop Bildverarbeitung für die Medizin 2006 Algorithmen - Systeme - Anwendungen*, Hamburg, pp 11-15, 2006.
9. K. Chaisaowong, P. Jäger, S. Vogel, A. Knepper, T. Kraus, and T. Aach, "Computer-assisted diagnosis for early stage pleural mesothelioma: Automated extraction of pleura to detect pleural thickenings from thoracic CT images," in Proc. *International Workshop on Advanced Image Technology*, Bangkok, pp 229-234, 2007.
10. Q. Hu, Z. Hou, and W.L. Nowinski, "Supervised range-constrained thresholding," *IEEE Trans Image Process.* 15(1): 228-240, 2006.
11. A.C. Silva, P.C.P. Carvalho, and R.A. Nunes, "Segmentation and reconstruction of the pulmonary parenchyma," *In-house technical report*, Vision and Graphics Laboratory, Instituto Nacional de Matemática Pura e Aplicada, Brazil, 2002.
12. C.B. Barber, D.P. Dobkin, and H. Huhdanpaa, "The quickhull algorithm for convex hulls," *ACM TOMS.* 22(4):469–483, 1996.
13. F.L. Bookstein, "Shape and information in medical images: A decade of morphometric synthesis," *CVIU*. 66(2): 97-118, 1997.
14. W.E. Lorensen and H.E. Cline, "Marching cubes: A high resolution 3D surface construction algorithm," *Comput Graph.* (Proceedings of ACM SIGGRAPH) 21(4):163-169, 1987.
15. H. Morneburg, *Bildgebende Systeme für die medizinische Diagnostik*, Publicis MCD Verlag, 3 ed., Erlangen, 1995.
16. Bernd Jähne, *Digital Image Processing*, Springer-Verlag, Berlin, Heidelberg, 2005.
17. N. Otsu, "A threshold selection method from gray-level histograms," *IEEE Trans. Syst., Man, Cybern.*, SMC-9(1):62–66, 1979.
18. A. Rosenfeld, and P. De la Torre, "Histogram concavity analysis as an aid in threshold selection," *IEEE Trans. Syst. Man Cybern.*, SMC-13:231-235, 1983.